Applied Surface Science 362 (2016) 49–55

Contents lists available at ScienceDirect

Applied Surface Science

journal homepage: www.elsevier.com/locate/apsusc

The adhesion behavior of carbon coating studied by re-indentation during in situ TEM nanoindentation

Xue Fan, Dongfeng Diao*

Institute of Nanosurface Science and Engineering (INSE), Shenzhen University, Nanhai Ave. 3688, Shenzhen 518060, Guangdong, China

ARTICLE INFO

Article history:
Received 30 September 2015
Accepted 20 November 2015
Available online 25 November 2015

Keywords:
Adhesion
Re-indentation
Carbon coating
In-situ nanoindentation
Transmission electron microscope

ABSTRACT

We report a nanoscale adhesion induced nano-response in terms of re-indentation during in situ transmission electron microscope (TEM) nanoindentation on the carbon coating with silicon substrate. The adhesive force generated with nanoindentation was measured, and re-indentation phenomenon during unloading with displacement sudden drop and external loading force change from tension to compression was found. The occurrence of re-indentation during unloading was ascribed to the adhesive force of the contact interface between the indenter and the coating surface. Adhesion energies released for re-indentation processes were quantitatively analyzed from the re-indentation load–displacement curves, and carbon coating reduced the impact of adhesion for silicon substrate. The adhesion induced nano-response of contact surfaces would affect the reliability and performance of nano devices.

1. Introduction

Carbon coatings have brought bright prospect in the development of nano devices, since the unique carbon structure of graphene, fullerene, carbon nanotube results in a combination of desirable mechanical [1], tribological [2,3], electrical [4], magnetical [5,6], and optical [7] properties. For its application on novel functional carbon based nano devices, the adhesive force at two contacted solid surfaces plays an essential role to determine the performance of nano devices, for example the tribotronic devices [8] convert the mechanical energy from contact-separation or relative movement into electricity or electrostatic potential [9,10], while adhesion between two material surfaces will prevent relative motion [11]. The adhesive force can be large enough to have influences at nanoscale contact on biological samples [12] and polymer films [13]. Therefore, it is important to study the adhesive properties of the coating surface as well as the adhesion induced nano-response in terms of any sudden movement at nanoscale.

The study of adhesion was often extracted from the pull-off force for tips in contact with flat substrates by means of atomic force microscope (AFM) measurements [14–16] or theoretical molecular dynamics (MD) simulations [17–19]. Such contact does not involve in the elastic-plastic deformations. During nanoindentation contact, the indentation force results from the addition of adhesive and elastic forces at the indenter-sample contact [20,21]. As the critical indentation depth decreases to nanoscale, the effect of adhesion has to be considered [22]. In situ nanoindentation in transmission electron microscope (TEM) enables the real-time observation of deformation and simultaneous measurement of load–displacement behavior [23–27]. By using the in situ nanoindentation, the adhesion at the actual indent region can be measured and directly observed, which provides an effective way to study the adhesion of the two contact surface in nano devices. However, in situ observations of nanoscale adhesion on coating substrate have not been reported yet.

In this paper, we report an in situ TEM observation of adhesion induced re-indentation of carbon coating. The carbon coating was fabricated on silicon wedge substrate by electron cyclotron resonance (ECR) plasma sputtering. Focused ion beam was used to fabricate carbon coated silicon pillar specimens for in situ TEM nanoindentation tests, which were carried out in displacement controlled mode. The loading and unloading processes were in situ observed and the load–displacement curves were recorded. Re-indentation phenomena during unloading for the nano-response of adhesion was investigated and the adhesion energies of different re-indentation loops were quantitatively analyzed.

2. Experiments

2.1. Sample preparation

The carbon coating was prepared on a polished silicon wedge substrate (p-type ⟨1 0 0⟩) by the electron cyclotron resonance (ECR) plasma sputtering method [28]. Magnetic field and microwave

* Corresponding author. Tel.: +86 755 26902415.
E-mail address: dfdiao@szu.edu.cn (D. Diao).

http://dx.doi.org/10.1016/j.apsusc.2015.11.196
0169-4332/

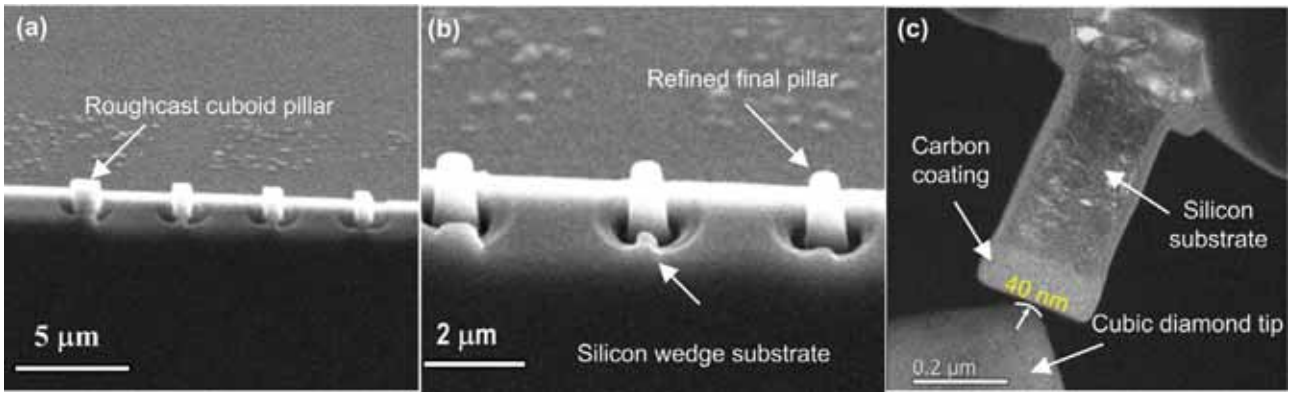

Fig. 1. (a) and (b) The FIB processing to fabricated carbon coated silicon pillar specimens for in situ nanoindentation tests with roughcasts pillar processing and refinement pillar processing, respectively. (c) The dark-field TEM image of the indenter and the carbon coated silicon pillar (coating thickness of 120 nm) before in situ nanoindentation test.

were combined to generate argon plasma. Silicon wedge substrate was pre-sputtered prior to deposition by 3 min etching to remove any residual contaminants. Then, carbon atoms were consequently sputtered off the target and carbon coatings with thickness of 120 nm and 20 nm were prepared by applying a substrate bias voltage. After coating deposition, the ECR carbon coating on silicon samples were micromachined to pillar specimens for in situ nanoindentation tests by using a FEI Helios Nanolab 600 focused ion beam (FIB). First, the sample was FIB milled to rectangle roughcasts pillar with an initial geometry of 500 nm in width, 500 nm in thickness and 800 nm in length, as shown in Fig. 1(a). During this stage, 30 kV ion accelerating voltage and 93 nA FIB current was applied. Then take coating thickness and pillar specimen size into consideration, two pillar specimen of different sizes were processed by refinement operation and fine machining under 15 kV ion accelerating voltage and 43 pA FIB current. Coating with 20 nm thickness had dimensions of 250 nm × 250 nm × 720 nm, and coating with 120 nm thickness had dimensions of 250 nm × 250 nm × 450 nm, respectively, the latter one observed by scanning electron microscope is shown in Fig. 1(b). One thing should be noticed that ultralow FIB current of 43 pA was applied during the finishing stage to avoid possible damages (including ion doping) or thermal recrystallization caused by ion bombardments.

2.2. In-situ nanoindentation

In situ nanoindentation tests were carried out inside a JEOL JEM-2100F TEM using the Hysitron PI95 PicoIndenter. A Boron-through-doped diamond cube corner indenter with curvature radius of 40 nm was used. The experiments were run in displacement controlled mode due to its sensitivity to transient phenomenon. For this purpose, a miniature capacitive load–displacement transducer was integrated into the TEM holder, which permitting high-resolution measurements of the load–displacement response (resolution of <3 nN in load, <0.02 nm in displacement). Fig. 1(c) shows the dark-field TEM image of the indenter and the carbon coated silicon pillar. Before the in situ nanoindentation test, the cubic diamond tip was carefully adjusted to make sure that the tip can perpendicularly indent on the carbon coated silicon pillar specimen. The nanoindentation tests were conducted at a controlled displacement rate in the range of 2 to 5 nm/s. To investigate the adhesion induced nano-response in the load–displacement curves, two different maximum indentation depths h_{max} (85 nm and 135 nm) were performed on the carbon coating with thickness of 120 nm, which presented the depth smaller and larger than the coating thickness. For coating with thickness of 20 nm, only one depth of 85 nm was chosen to perform the test. The corresponding structural evolution was recorded with a Gatan 830 (SC200) CCD camera.

3. Results

The displacement and load variations with maximum indentation depth of 85 nm on the 120 nm ECR carbon coating were shown in Fig. 2. As shown in Fig. 2(a), during the unloading process, two sudden displacement drops were found and the load decreased to negative values at the same time. The displacement drops implied that the tip experienced from getting rid of contact to re-contact with the sample. Checking the load–displacement curves in Fig. 2(b), it is interesting to note that two re-indentation loops during unloading were detected. For the first re-indentation, the position of the indenter moved a distance, from 33.4 nm to 19.3 nm and to 28.4 nm at last in the very short time, correspondingly, the external loading force (P) applied on the indenter changed from −8.7 μN to 0 μN, and finally to 1.7 μN. The other re-indentation started at indentation depth of 18.1 nm, and the re-indentation load is too small to be clearly observed.

Fig. 3(a)–(f) shows the TEM images during the in situ nanoindentation tests, in one-to-one correspondence with the six points A-F marked in its load–displacement curve displayed in Fig. 2(b). Fig. 3(a) shows the initial aspect before the test. Fig. 3(b) corresponds with the maximum indentation depth h_{max} of 85 nm, where the value of P was 285.4 μN. It could be found that plastic deformation was initiated at the coating surface. At indentation depth of 33.4 nm during unloading (Fig. 3(c)), the loading force exhibited a negative value of −8.7 μN, which was generated by the adhesive force between the tip and the coating. Through Fig. 3(c)–(e), a clear discontinuity in the unloading curve can be observed, and the displacement suddenly dropped followed by moving back. Note that this process took about 0.1 s, in which the external loading force changed from tension to compression as indicated by red dotted arrow in Fig. 2(b) and one loop of re-indentation process occurred. The other re-indentation process started at 18.1 nm of indentation depth, most evident in Fig. 2(a). After complete unloading in this test, a final coating deformation of 20.0 nm was detected from the bright-field TEM image of Fig. 3(f). The whole in situ nanoindentation process was shown from the Supplementary movie M1.AVI.

For the ECR carbon coating with thickness of 120 nm, the other nanoindentation test with the maximum indentation depth h_{max} of 135 nm was performed. The load and displacement versus time are shown in Fig. 4(a), and we can see three displacement sudden drops, correspondingly, the external loading force fluctuated. Fig. 4(b) shows the load–displacement curve, and three obvious re-indentation loops can be found. The re-indentation processes

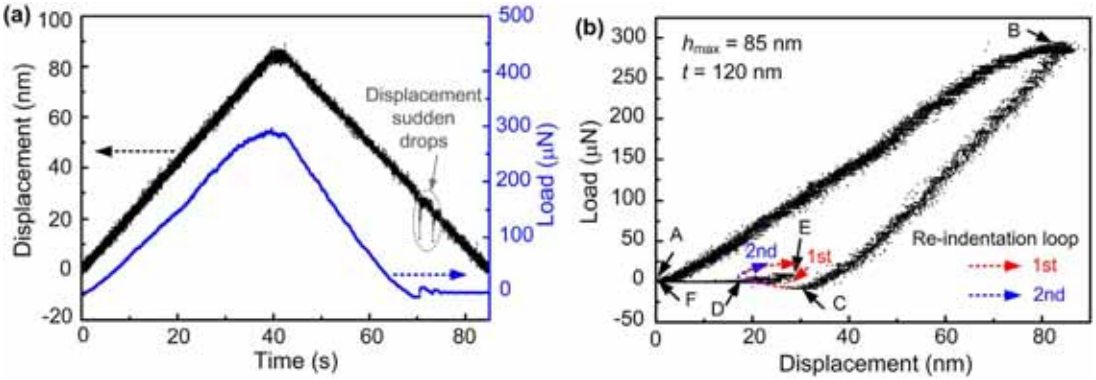

Fig. 2. Displacement and load variations during the in situ nanoindentation process with maximum indentation depth of 85 nm (coating thickness of 120 nm). (a) Displacement and load versus time, (b) Load–displacement curve. (For interpretation of the references to color in this figure legend, the reader is referred to the web version of this article.)

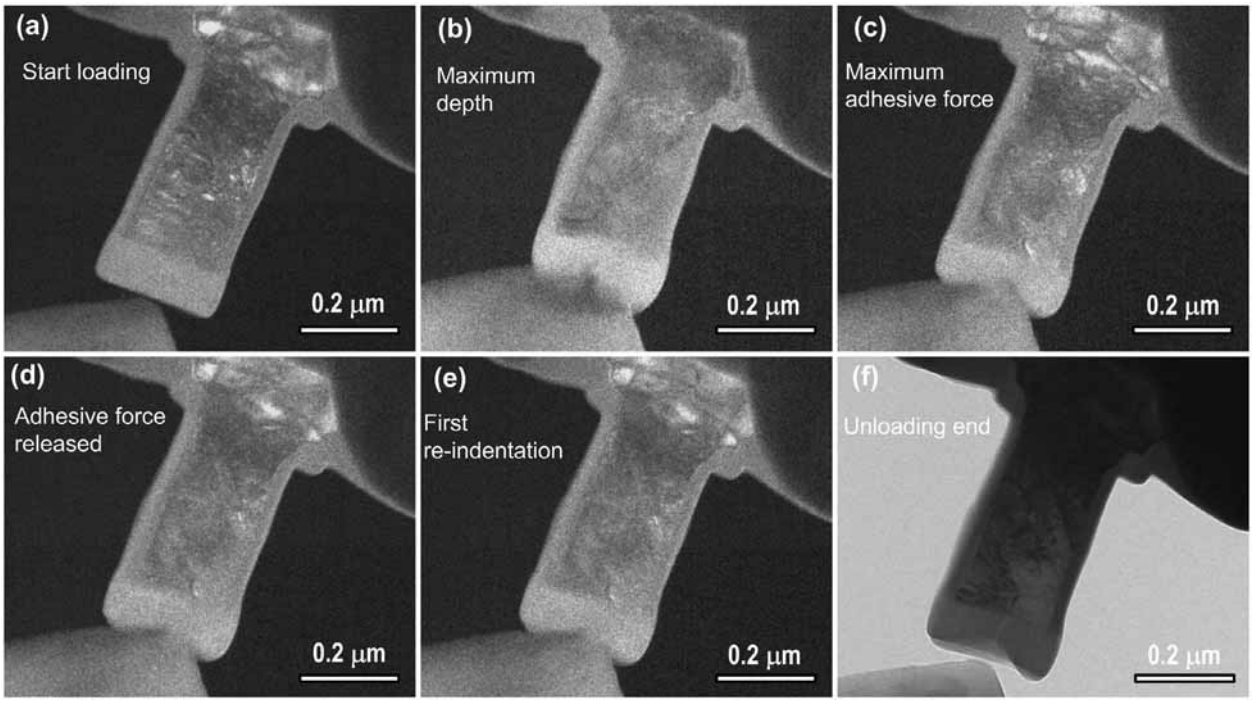

Fig. 3. (a)–(e) video montages taken from the dark-field TEM movie with maximum indentation depth of 85 nm (coating thickness of 120 nm), (f) bright-field TEM image after the test. (a)–(f) were in one-to-one correspondence with the six points A–F in its load–displacement curve in Fig. 2(b).

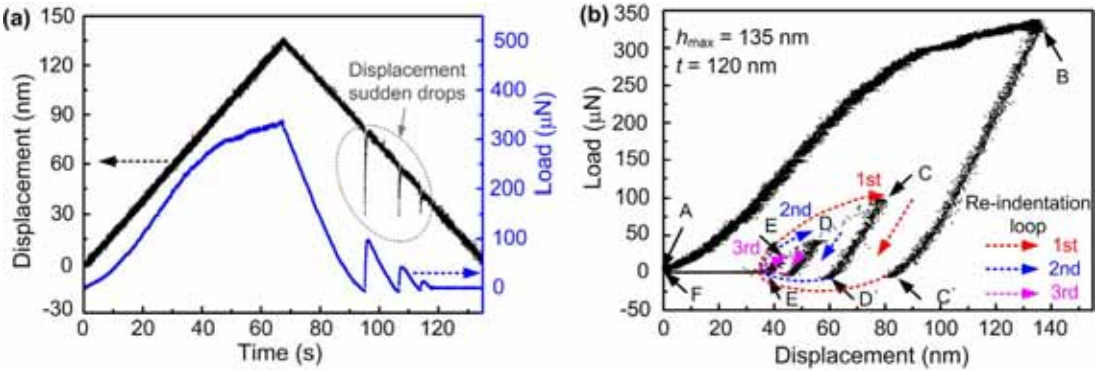

Fig. 4. Displacement and load variations during the in situ nanoindentation process with maximum indentation depth of 135 nm (coating thickness of 120 nm). (a) Displacement and load versus time, (b) Load–displacement curve.

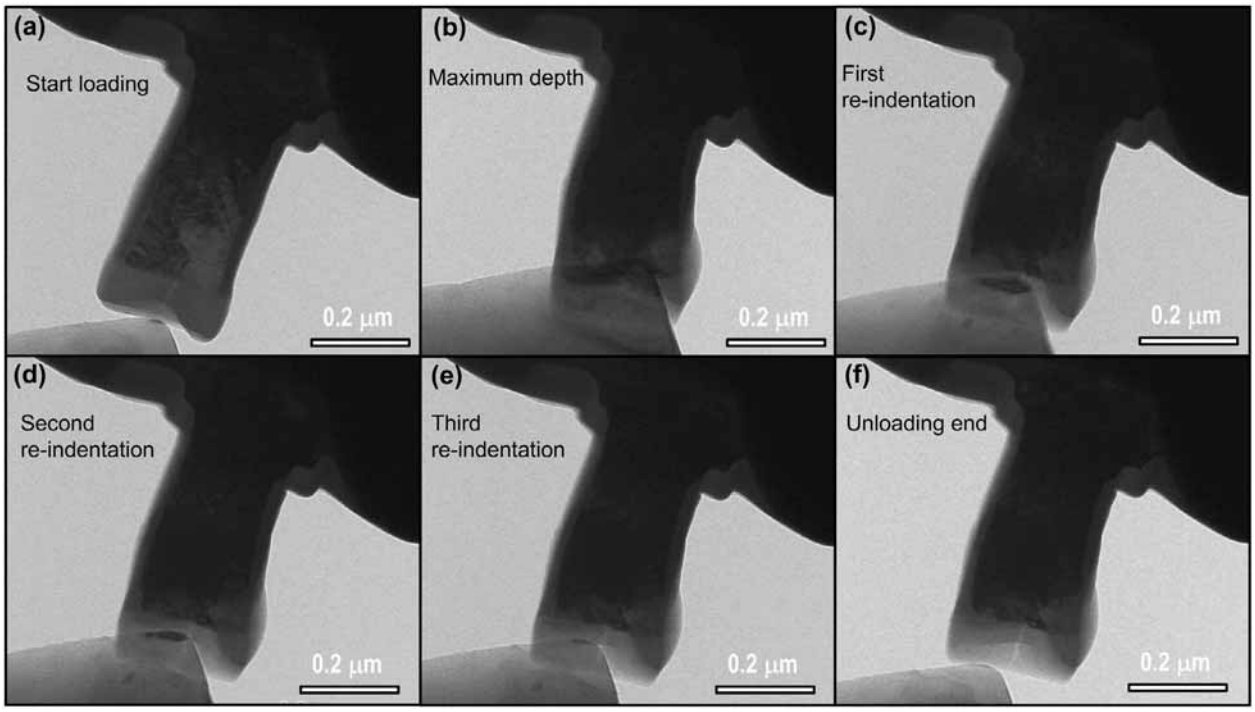

Fig. 5. Six representative in situ nanoindentation states taken from the bright-field TEM movie with maximum indentation depth of 135 nm (coating thickness of 120 nm), (a)–(f) were in one-to-one correspondence with the six points A–F marked in its load–displacement curve in Fig. 4(b).

started with the adhesive force of −6.1 μN, −8.3 μN and −4.4 μN for the first, second and third loop, respectively, as indicated with C', D' and E' in the figure. Six representative TEM images in one-to-one correspondence with the six points A–F marked in Fig. 4(b) were shown in Fig. 5. Through Fig. 5(a) and (b), the indentation depth increased gradually without breaking the pillar specimen. Fig. 5(b) corresponds with h_{max} of 135 nm, and the force applied on the indenter got the maximum value of 335 μN. Fig. 5(c)–(e) exhibited the re-loading to maximum re-indentation depth states for the three re-indentation loops, and the maximum re-indentation depth gradually decreased. A high contrast dark region below the apex of tip was observed in Fig. 5(c)–(e), the contrast in this localized region is attributed to the large strain gradients underneath the indenter during re-indentation process. It is suggested that the region under compression are denser, then the scattering of the incident electron beam is greater and the contrast is darker [24]. The darker contrast region decreased with the re-indentation loop increased, which means the re-indentation induced compression decreased with time increase. The value of final coating deformation was 35 nm as shown in Fig. 5(f), and a crack was observed in the middle of carbon coating. Supplementary movie M2.AVI shows the dynamic process of in-situ nanoindentation. Compared with the test results in Fig. 2, the number of re-indentation loop increased, while the maximum adhesive force to start a re-indentation barely changed. All the forces were less than −10 μN for the 120 nm carbon coating.

To confirm the re-indentation nano-response induced by adhesion release during unloading, in situ nanoindentation test was carried out on the other ECR carbon coating with a much thinner thickness of 20 nm. Since the film is too thin that cannot be avoided by the substrate effect with smaller indentation depth, only one maximum indentation depth of 85 nm was chosen to perform the in situ nanoindentation test. Fig. 6 shows the load and displacement variations. During the loading process, with the indentation depth increase, the external loading force gradually increased until a sudden load drop happened as shown in Fig. 6(a). The coating was fractured, which is most evident in correspondence to the clear discontinuity of load–displacement curve in Fig. 6(b). With the displacement further increased, a pop-in feature can be observed in the loading curve which is related to the delamination of a large part of the coating [1]. When the indentation depth reached the maximum value of 85 nm, the external loading force was 99.8 μN. During unloading, displacement sudden drops, which corresponded to the re-indentation processes, were also found. The first large displacement drop occurred at around 60 nm indentation depth, and the other two smaller drops occurred when the indentation depth was 45.9 nm and 38.0 nm, respectively. The dynamic nanoindentation process was shown from the Supplementary movie M3.AVI.

Fig. 7 shows the bright-field TEM images of in situ nanoindentation test, in one-to-one correspondence with the nine points A-I marked in its load–displacement curve displayed in Fig. 6(b). The initial aspect before the test was shown in Fig. 7(a). Fig. 7(b) shows that the external loading force (P) reached the maximum value for the first time in the middle of loading process, the coating was not penetrated when the indention depth was at 50 nm. With the working of displacement controller, the displacement of the indenter kept increasing and the coating was suddenly fractured, which corresponded with the clear discontinuity of load–displacement curve (See point C in Fig. 6(b) and relative Fig. 7(c)). The discontinuity in loading curve was ascribed to the fracture of thin carbon coating. After the coating fracture, a pop-in feature can be observed in the loading curve which may relate to the delamination of a large part of the coating, as shown from Fig. 7(d) to (e). Fig. 7(f) corresponded to the maximum indentation depth h_{max} of 85 nm. Due to the fracture and delamination of carbon coating, an obvious elastic-plastic deformation can be observed. From Fig. 7(g) to (h), the external loading force jumped from negative value to a positive one very quickly in about 0.1 s, which resulted in the first re-indentation during unloading. According to the load–displacement curve, another two small re-indentations occurred after the first one. Finally, after the unloading process (as shown in Fig. 7(i)), coating fracture and the residual indentation depth which is much deeper than the coating thickness can be observed. One may note that the first displacement drop and relative adhesive force are much larger than

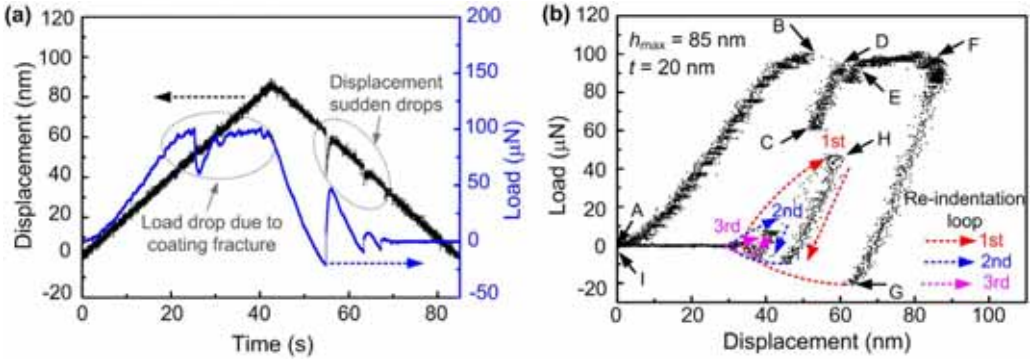

Fig. 6. Displacement and load variations during the in situ nanoindentation process with maximum indentation depth of 85 nm (coating thickness of 20 nm). (a) Displacement and load versus time; (b) Load–displacement curve.

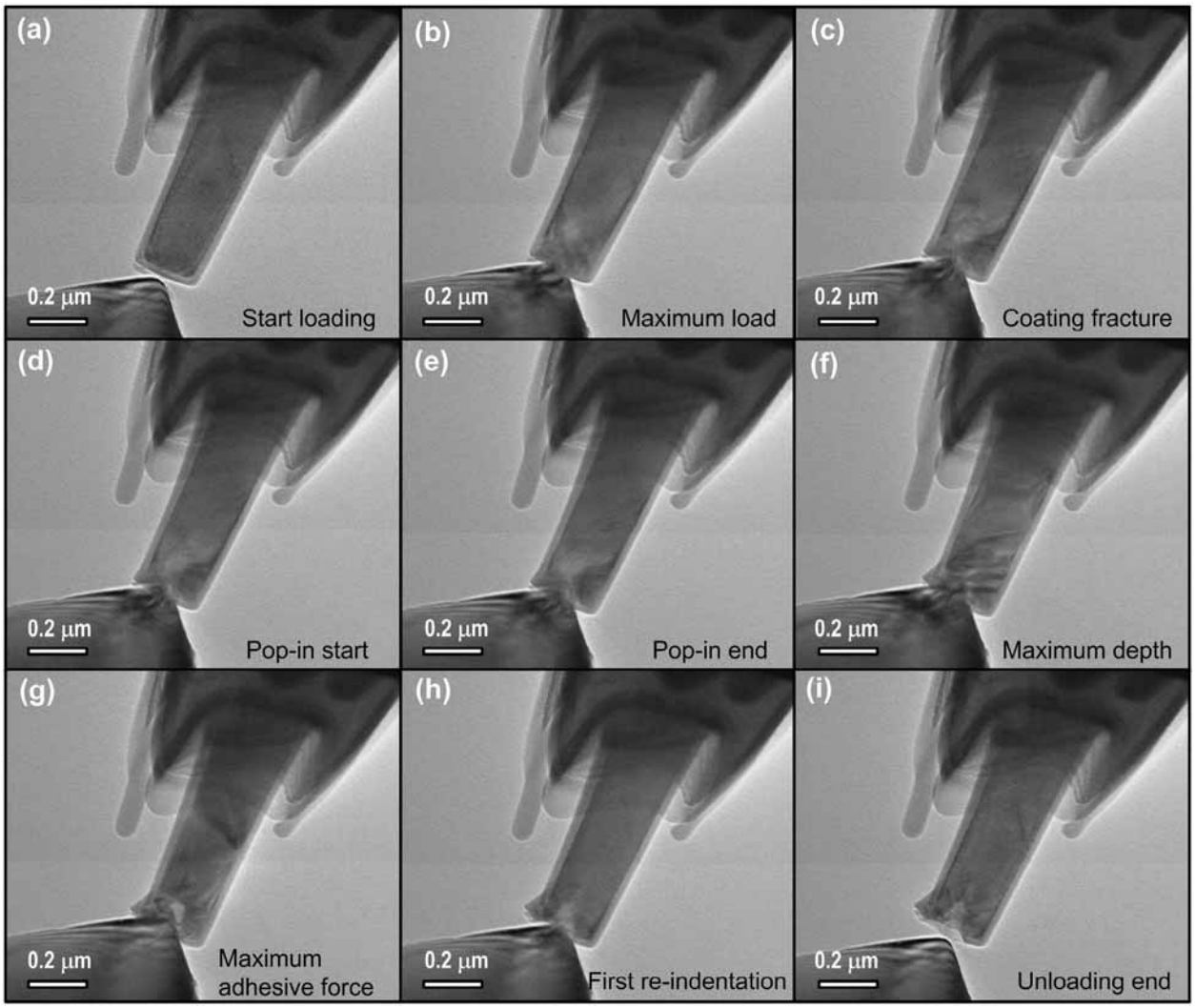

Fig. 7. In situ TEM nanoindentation of the carbon coating with thickness of 20 nm. Images (a)–(i) were video montages taken from the bright-field TEM movie during the nanoindentation test and corresponded to the numbered points A–I marked in the load–displacement curve in Fig. 6(b).

the other two re-indentations. The value of P was −20.8 μN, which is also much larger than the adhesive forces when the tip contact with 120 nm carbon coating. The reason is suggested that when part of thin carbon coating is delaminated, the indenter contacts directly with the silicon substrate, and the adhesive force between diamond tip and silicon is larger than that when the indenter only contact with the carbon coating, which will be analyzed next.

4. Discussion

In the aim of clearly exhibit how adhesion induced a re-indentation nano-response, and how it was captured with the in-situ TEM nanoindentation test in displacement controlled mode, three working states of the miniature capacitive load–displacement transducer during unloading were presented in Fig. 8. Taken the

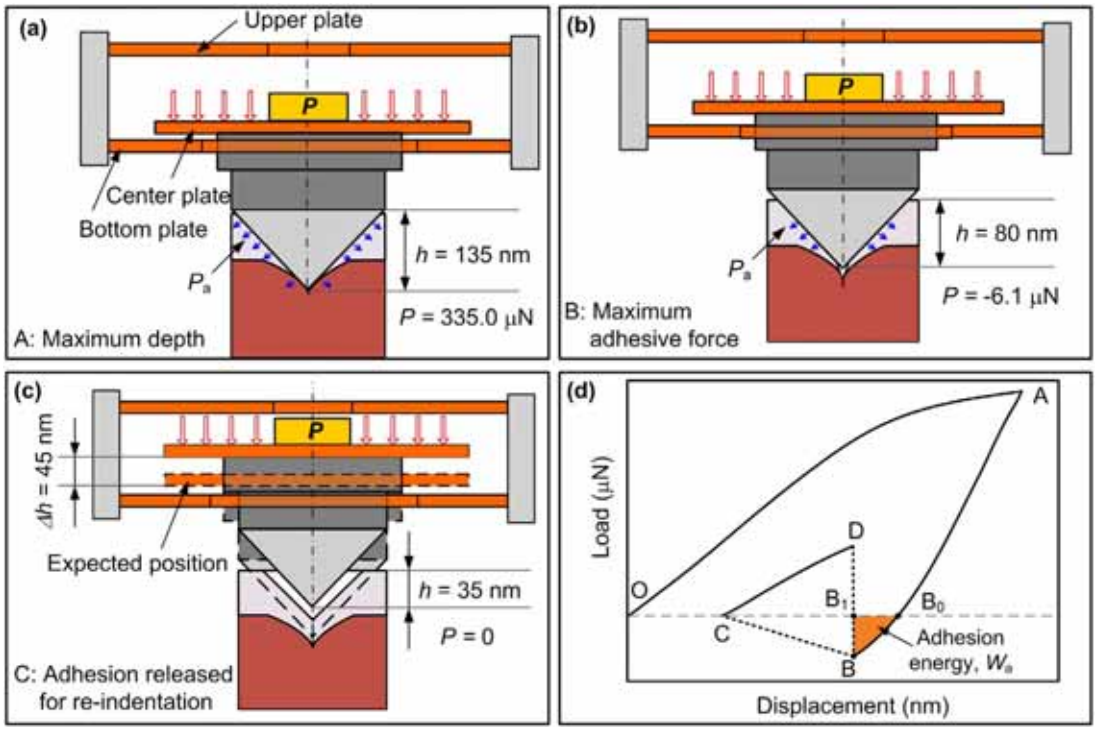

Fig. 8. Schematic of three working states during unloading process for 120 nm carbon coating with maximum indentation depth of 135 nm (a) The starting point of unloading at depth of 135 nm, (b) The maximum adhesion point at depth of 80 nm, (c) The starting point of re-indentation at depth of 35 nm, (d) The corresponding schematic load–displacement curve contains the loading, unloading and first re-indentation processes.

Table 1
The adhesion energies stored in different re-indentation processes during unloading.

In-situ TEM nanoindentation		Adhesion energy W_a ($\times 10^{-15}$ J)		
Coating thickness t (nm)	Maximum indentation depth h_{max} (nm)	1st loop	2nd loop	3rd loop
120	85	1003.4	747.9	–
120	135	20,244.8	19,486.1	4330.1
20	85	100,800.0	17,310.3	7149.0

first re-indentation occurred on the 120 nm ECR carbon coating with h_{max} of 135 nm for example, Fig. 8(a) shows the working state at the maximum indentation depth (135 nm). The external loading force (P of 335.0 μN) contained the actions of the elastic force and the adhesive force P_a, which resulted from the adhesion between the indenter and the carbon coating on silicon. When the indentation depth is reduced to 80 nm as shown in Fig. 8(b), the elastic deformation was recovered and the adhesive force became the largest in this position, as a sum, P got the value of −6.1 μN. Through Fig. 8(b) to (c), due to the sudden disappearance of adhesive force, the indenter tip jumped back 45 nm, from 80 nm to 35 nm, along unloading direction. According to the one-to-one relationship between the displacement of the indenter tip and the external loading force applied, the indenter has to move back from 35 nm to 80 nm. Thereafter, the nano-response of adhesion resulted in a re-indentation during unloading, which was detected by our in situ TEM nanoindentation tests in displacement controlled mode.

In order to further recognize the adhesion induced re-indentation, the energy released in adhesion was quantitatively analyzed. Since the area under the load–displacement curve is the work performed by the indenter during elastic-plastic deformation of carbon coated silicon substrate [29]. In our experiments, the energy transformation between two different loops of re-indentation (adhesion energy) during unloading can be calculated from the corresponding areas in the unloading curve. Fig. 8(d) shows a simplified load–displacement curve containing the loading (OA), unloading (AB), and the first re-indentation (BCD). Let us consider the unloading curve ABCD. During the unloading process, the pure elastic deformation was recovered at point B_0, where P reduced to zero and the compression effect by indenter disappeared. However, due to the adhesion between tip and nanosurface, the displacement of indenter kept moving from B_0 to B, and the adhesion accumulated to the maximum. Then, after the adhesion energy was released, the indenter showed up a sudden displacement jump to C and a re-indentation process to D. Therefore, the adhesion energy stored for this re-indentation process should be the area of B_0BB_1 (W_a), as shown in Fig. 8(d). It can be noted that the adhesion energy stored for different re-indentation loops is different. Table 1 shows the analyzed adhesion energy for all of the re-indentations occurred with different loops during unloading. It can be seen that as the loop of re-indentation increases, the adhesion energy gradually decreased. For the ECR carbon coating with thickness of 120 nm, the coating was not delaminated during the whole in situ nanoindentation process, and the adhesion energies between diamond tip and carbon coating were relative small. When the carbon coating (thickness of 20 nm) is fractured and delaminated during nanoindentation, the indenter contacts directly with the silicon substrate, at this time, the adhesion energy ($100{,}800.0 \times 10^{-15}$ J) is at least five times larger than the case that the indenter only contact with the ECR carbon coating. This means that ECR carbon coating plays an important role in decreasing the surface adhesion energy for silicon substrate.

5. Conclusion

In this paper, to explore the nano-response induced by nanoscale adhesion at the carbon coated surface, we performed in situ TEM nanoindentation test. The re-indentation phenomenon with displacement sudden drop and external loading force change from tension to compression was directly observed. The origin of re-indentation was ascribed to the adhesion of the contact interface between the indenter and the coating surface. The adhesion energies stored in the re-indentation processes were quantitatively calculated from the re-indentation load–displacement curves. Results showed that the adhesion energy between tip-carbon is one fifth smaller than that between tip-silicon, carbon coating reduce the impact of adhesion induced nano-response for silicon substrate. This research brings about an adhesion induced nano-response in terms of re-indentation with different adhesive forces and energies, which impact the reliability and performance of nano devices.

Acknowledgements

The authors would like to acknowledge the National Natural Science Foundation of China (No. 51305332 and No. 51575359), the Young-Researcher-Starting grant of Shenzhen University (No. 201526). And the authors are very grateful to Dr. Pengyu Zhang for supporting the experiments, Prof. Zhiwei Shan of Xi'an Jiaotong University for his help in arranging experimental equipments, and Prof. Xiaodong Li of University of Virginia for his help in discussing the mechanism of re-indentation.

Appendix A. Supplementary data

Supplementary data associated with this article can be found, in the online version, at http://dx.doi.org/10.1016/j.apsusc.2015.11.196.

References

[1] X. Fan, K. Nose, D.F. Diao, T. Yoshida, Nanoindentation behaviors of amorphous carbon films containing nanocrystalline graphite and diamond clusters prepared by radio frequency sputtering, Appl. Surf. Sci. 273 (2013) 816–823.
[2] J. Umeda, B. Fugetsu, E. Nishida, H. Miyaji, K. Kondoh, Friction behavior of network-structured CNT coating on pure titanium plate, Appl. Surf. Sci. 357 (2015) 721–727.
[3] Y.F. Wang, J.M. Guo, K.X. Gao, B. Zhang, A.M. Liang, J.Y. Zhang, Understanding the ultra-low friction behavior of hydrogenated fullerene-like carbon films grown with different flow rates of hydrogen gas, Carbon 77 (2014) 518–524.
[4] C. Wang, D.F. Diao, X. Fan, C. Chen, Graphene sheets embedded carbon film prepared by electron irradiation in electron cyclotron resonance plasma, Appl. Phys. Lett. 100 (2012) 231909.
[5] X. Zhang, C. Wang, C.Q. Sun, D.F. Diao, Magnetism induced by excess electrons trapped at diamagnetic edge-quantum well in multi-layer graphene, Appl. Phys. Lett. 105 (2014) 042402.
[6] C. Wang, X. Zhang, D.F. Diao, Nanosized graphene crystallite induced strong magnetism in pure carbon films, Nanoscale 7 (2015) 4475–4481.
[7] M. Shakerzaheh, N. Xu, M. Bosman, B.K. Tay, X. Wang, E.H.T. Teo, H. Zheng, H. Yu, Field emission enhancement and microstructural changes of carbon films by single pulse laser irradiation, Carbon 49 (2011) 1018–1024.
[8] C. Zhang, W. Tang, L. Zhang, C. Han, Z.L. Wang, Contact electrification field-effect transistor, ACS Nano 8 (2014) 8702–8709.
[9] S. Wang, L. Lin, Z.L. Wang, Triboelectric nanogenerators as self-powered active sensors, Nano Energy 11 (2015) 436–462.
[10] Z.L. Wang, Triboelectric nanogenerators as new energy technology for self-powered systems and as active mechanical and chemical sensors, ACS Nano 7 (2013) 9533–9557.
[11] F.W. DelRio, B.M.P. De, J.A. Knapp, E.D. Reedy, P.J. Clews, M.L. Dunn, The role of van der Waals forces in adhesion of micromachined surfaces, Nat. Mater. 4 (2005) 629–634.
[12] Y. Rabinovich, M. Esayanur, S. Daosukho, K. Byer, H. El-Shall, S. Khanc, Atomic force microscopy measurement of the elastic properties of the kidney epithelial cells, J. Colloid Interface Sci. 285 (2005) 125–135.
[13] Y.P. Zhao, X. Shi, W.J. Li, Effect of work of adhesion on nanoindentation, Rev. Adv. Mater. Sci. 5 (2003) 348–353.
[14] J. Grobelny, N. Pradeep, D.I. Kim, Z.C. Ying, Quantification of the meniscus effect in adhesion force measurements, Appl. Phys. Lett. 88 (2006) 091906.
[15] X. Fenga, B.D. Kievieta, J. Songb, P.M. Schöna, G.J. Vancso, Adhesion forces in AFM of redox responsive polymer grafts: effects of tip hydrophilicity, Appl. Surf. Sci. 292 (2014) 107–110.
[16] Z. Chai, Y. Liu, X. Lu, D. He, Reducing adhesion force by means of atomic layer deposition of ZnO films with nanoscale surface roughness, ACS Appl. Mater. Interfaces 6 (2014) 3325–3330.
[17] K.E. Ryan, P.L. Keating, T.D.B. Jacobs, D.S. Grierson, K.T. Turner, R.W. Carpick, J.A. Harrison, Simulated adhesion between realistic hydrocarbon materials: effects of composition, roughness, and contact point, Langmuir 30 (2014) 2028–2037.
[18] J. Blass, M. Albrecht, B.L. Bozna, G. Wenz, R. Bennewitz, Dynamic effects in friction and adhesion through cooperative rupture and formation of supramolecular bonds, Nanoscale 7 (2015) 7674–7681.
[19] B.Q. Luan, M.O. Robbins, Contact of single asperities with varying adhesion: comparing continuum mechanics to atomistic simulations, Phys. Rev. E: Stat. Nonlinear Soft Matter Phys. 74 (2006) 026111.
[20] L. Sirghi, F. Rossi, Adhesion and elasticity in nanoscale indentation, Appl. Phys. Lett. 89 (2006) 243118.
[21] L. Sirghi, F. Rossi, The effect of adhesion on the contact radius in atomic force microscopy indentation, Nanotechnology 20 (2009) 365702.
[22] L. Li, W. Song, M. Xu, A. Ovcharenko, G. Zhang, Atomistic insights into the loading-Unloading of an adhesive contact: a rigid sphere indenting a copper substrate, Comp. Mater. Sci. 98 (2015) 105–111.
[23] A.M. Minor, S.A.S. Asif, Z. Shan, E.A. Stach, E. Cyrankowski, T.J. Wyrobek, O.L. Warren, A new view of the onset of plasticity during the nanoindentation of aluminium, Nat. Mater. 5 (2006) 697–702.
[24] J. Zhou, K. Komvopoulos, A.M. Minor, Nanoscale plastic deformation and fracture of polymers studied by in situ nanoindentation in a transmission electron microscope, Appl. Phys. Lett. 88 (2006) 181908.
[25] D.S. Wang, S.Y. Chang, Y.C. Huang, J.B. Wu, H.J. Lai, M.S. Leu, Nanoscopic observations of stress-induced formation of graphitic nanocrystallites at amorphous carbon surfaces, Carbon 74 (2014) 302–311.
[26] C. Iwamoto, H.S. Yang, S. Watanabe, T. Yoshida, Dynamic and atomistic deformation of sp2-bonded boron nitride nanoarrays, Appl. Phys. Lett. 83 (2003) 4402–4404.
[27] S. Ii, C. Iwamoto, K. Matsunage, T. Yamamoto, Y. Ikuhara, TEM in situ observation of fracture behavior in ceramic materials, Appl. Surf. Sci. 241 (2005) 68–74.
[28] X. Fan, D.F. Diao, K. Wang, C. Wang, Multi-functional ECR plasma sputtering system for preparing amorphous carbon and Al—O—Si films, Surf. Coat. Technol. 206 (2011) 1963–1970.
[29] X.D. Li, D.F. Diao, B. Bhushan, Fracture mechanisms of thin amorphous carbon films in nanoindentation, Acta Mater. 45 (1997) 4453–4461.